

Cotunneling, current blockade, and backaction forces in nanobeams close to the Euler buckling instability

Guillaume Weick* and Dominique M.-A. Meyer

*Institut de Physique et Chimie des Matériaux de Strasbourg (UMR 7504),
CNRS and Université de Strasbourg, 23 rue du Loess, BP 43, F-67034 Strasbourg Cedex 2, France*

Single-electron transistors embedded in a vibrating nanoresonator such as a doubly-clamped carbon nanotube exhibit effects stemming from the coupling between electronic and vibrational degrees of freedom. In particular, a capacitive electromechanical coupling induces a blockade of the current at low bias voltage. It has been recently shown theoretically within a sequential-tunneling approximation that this current blockade can be enhanced by orders of magnitude when the suspended structure is brought to the Euler buckling instability. Here, we investigate the role of cotunneling on the predicted enhancement and show that the latter is not suppressed by cotunneling effects. We further demonstrate that despite the fact that the current blockade is difficult to measure far from the Euler instability, the backaction of the current flow on the nanobeam frequency may be easier to observe.

PACS numbers: 73.63.-b, 85.85.+j, 63.22.Gh

I. INTRODUCTION

Nanoelectromechanical systems^{1–4} exhibit effects originating from the coupling between electronic and vibrational degrees of freedom that go beyond the ones encountered in more conventional nanostructures such as quantum dots. A prominent example of these new effects is the low-bias current blockade induced by a capacitive electromechanical coupling when a single-electron transistor is embedded in a vibrating structure.⁵ This phenomenon is the classical counterpart of the Franck-Condon blockade in molecular devices^{6,7} that has been observed in suspended carbon nanotubes for high-energy vibrational modes.⁸ For low-energy (classical) vibrations, the blockade is difficult to observe due to the relatively weak electromechanical coupling typically encountered in experiments. However, it has been reported that this capacitive coupling is responsible for the modification of the flexural vibration frequency when electrons tunnel on a suspended carbon nanotube.^{9,10}

In Ref. 11, a way of enhancing the classical current blockade by orders of magnitude by exploiting the well-known Euler buckling instability¹² has been recently proposed: The energy scale associated with the bias voltage below which transport is blocked is given by⁵ $E_E = F_e^2/m\omega^2$, where F_e is the electromechanical coupling resulting from the gate capacitance of the device and ω and m the vibrational frequency and mass of its mechanical part, respectively. When a lateral compressive force F is exerted on a nanobeam forming a quantum dot coupled through tunnel barriers to source and drain reservoirs and capacitively coupled to a gate electrode as sketched in Fig. 1, its vibrational frequency ω goes down to zero when F reaches the critical force F_c at which buckling occurs.¹² Thus, one expects a large enhancement of the bias window below which current through the device is suppressed. The argument above would in principle suggest that the energy scale E_E diverges at the instability. However, anharmonicities in the vibrations of

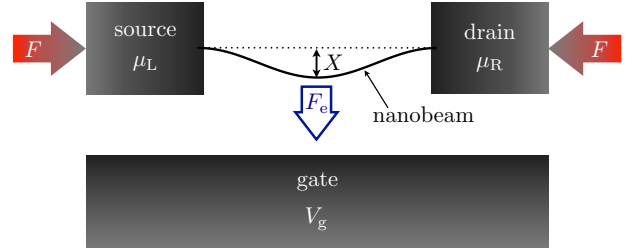


FIG. 1. (Color online) Sketch of the setup: a suspended doubly-clamped nanobeam (e.g., a carbon nanotube) with deflection amplitude X forming a quantum dot connected via tunnel barriers to source and drain electron reservoirs held at chemical potentials μ_L and μ_R by the bias voltage V , respectively. The nanobeam is capacitively coupled to a metallic electrode kept at a gate voltage V_g , which induces a stochastic force F_e that attracts the beam towards the gate electrode whenever the quantum dot is charged. The additional compression force F acts on the nanobeam and induces the buckling instability.

the nanobeam, which become crucial close to the Euler instability, cut off the apparent divergence.¹¹

First studied by Leonhard Euler in 1744 while investigating the maximal load that a column can sustain,¹³ the buckling instability is a paradigm for a continuous mechanical instability.¹² It has been the subject of various experimental studies in micro- and nanomechanical systems over the past years.^{14–18} In particular, buckling instabilities have been observed in carbon nanotubes^{14,15} and in SiO₂ nanobeams^{16,17} where it was demonstrated that, despite the small size of these objects, the mechanical instability can be explained in terms of continuous classical elasticity theory. Micromechanical beams beyond the Euler instability were also proposed to serve as mechanical memories in Ref. 18. The quantum properties of nanobeams close to the Euler instability were theoretically studied in Refs. 19–23. In particular, these

systems were proposed to investigate zero-point fluctuations of a mechanical mode²⁰ or to serve as a mechanical qubit.^{22,23} The Euler instability has been recently theoretically considered in nanoelectromechanical systems²⁴ in the case where the electromechanical coupling F_e is negligible with respect to the intrinsic electron-phonon coupling.²⁵ It was shown in Ref. 24 that this intrinsic coupling changes qualitatively the nature of the instability, turning it into a discontinuous one.²⁶

The results of Ref. 11 where the enhancement of the current blockade at the Euler instability was predicted were obtained in the sequential-tunneling regime of weak coupling to the electron reservoirs, i.e., $\hbar\Gamma \ll k_B T$ with Γ the typical tunneling-induced width (or hybridization) of the dot energy levels and T the temperature, where cotunneling currents are exponentially suppressed. In this paper, we investigate the role played by cotunneling that dominates the current inside the Coulomb diamond and which becomes relevant in the opposite regime of strong coupling to the leads, i.e., $\hbar\Gamma \gg k_B T$. We show that the current blockade survives for hybridization to the leads smaller than the energy scale E_E set by the bias voltage below which current is suppressed. Moreover, we show that the backaction of the current flow on the mechanical part of the device leads to large current-induced frequency shifts of the nanobeam that may be easier to observe experimentally than the current blockade when the nanobeam is far from the mechanical instability.

The paper is organized as follows: We start by presenting our model in Sec. II. Section III describes the effective statistical description in terms of a current-induced Langevin process of the nanobeam that we use to solve the model. Results for the transport characteristics of the device are given in Sec. IV, while Sec. V presents our predictions concerning the backaction that the current flow exerts on the nanoresonator. We finally conclude in Sec. VI.

II. MODEL

The model we consider is sketched in Fig. 1: A suspended nanobeam forms a quantum dot connected to source and drain leads via tunnel barriers. A lateral compression force F is exerted on the nanotube and brings it to the Euler buckling instability when F reaches the critical force F_c .¹² The total Hamiltonian of the system reads

$$H = H_{\text{vib}} + H_{\text{SET}} + H_c, \quad (1)$$

where H_{vib} describes the flexural vibrations of the nanobeam, H_{SET} accounts for the electronic degrees of freedom of the single-electron transistor (SET) and H_c represents the coupling between the mechanical motion of the beam and the electrons residing on the quantum dot.

At sufficiently low temperature, only the lowest-energy bending mode of amplitude X is significantly populated,

and the resulting vibrational Hamiltonian in Eq. (1) takes the Landau-Ginzburg form^{11,19–24}

$$H_{\text{vib}} = \frac{P^2}{2m} + \frac{m\omega^2}{2}X^2 + \frac{\alpha}{4}X^4, \quad (2)$$

with P the conjugated momentum to X and m the mass of the mode. In Eq. (2),

$$\omega = \omega_0 \sqrt{1 - \frac{F}{F_c}} \quad (3)$$

denotes the compression force-dependent vibrational frequency of the fundamental bending mode of the beam, with ω_0 the corresponding frequency for vanishing compression force F . The anharmonicity parameter $\alpha > 0$ stabilizes the mode for $F > F_c$ ($\omega^2 < 0$) where the nanobeam buckles in one of the two metastable positions at $X = \pm\sqrt{-m\omega^2/\alpha}$. For $F < F_c$ ($\omega^2 > 0$), the nanobeam stays flat at $X = 0$. For clamped boundary conditions, one can express¹¹ $F_c = \kappa(2\pi/L)^2$, $\omega_0 = \sqrt{\kappa/\sigma}(2\pi/L)^2$, $m = 3\sigma L/8$ and $\alpha = F_c L(\pi/2L)^4$ in terms of the bending rigidity κ , the length L and the linear mass density σ of the beam.

The single-electron transistor is modelled by the Hamiltonian

$$H_{\text{SET}} = H_{\text{dot}} + H_{\text{leads}} + H_{\text{tun}}, \quad (4)$$

with

$$H_{\text{dot}} = (\epsilon_d - e\bar{V}_g)n_d \quad (5)$$

the Hamiltonian describing the single-level quantum dot of energy ϵ_d , where $\bar{V}_g = C_g V_g / C_\Sigma$ is the (effective) gate voltage which is expressed in terms of the applied gate voltage V_g , the capacitance of the gate electrode C_g and the total capacitance C_Σ of the device. The occupation operator reads $n_d = d^\dagger d$ where d^\dagger (d) creates (annihilates) an electron on the dot. We consider for simplicity spinless electrons, as the inclusion of spin as well as on-site Coulomb repulsion in Eq. (5) should not qualitatively change our results. The electrons in the left (L) and right (R) reservoirs are considered to constitute Fermi liquids. The corresponding Hamiltonian reads

$$H_{\text{leads}} = \sum_{ka} (\epsilon_k - \mu_a) c_{ka}^\dagger c_{ka}, \quad (6)$$

where c_{ka}^\dagger (c_{ka}) creates (annihilates) an electron of momentum k with energy ϵ_k in lead $a = \text{L, R}$. The lead a is maintained at the chemical potential μ_a by the bias voltage V , such that $\mu_L - \mu_R = eV$. In what follows, we assume the voltage drop across the junction to be symmetric, i.e., $\mu_L = -\mu_R = eV/2$. Tunneling between the quantum dot and the left and right leads is accounted for by the Hamiltonian

$$H_{\text{tun}} = \sum_{ka} (t_a c_{ka}^\dagger d + t_a^* d^\dagger c_{ka}), \quad (7)$$

with t_a the tunneling amplitude between the dot and lead a .

The flexural vibrations of the nanobeam couple to electronic transport due to the gate electrode that exerts the electrostatic force $-F_e$ when the quantum dot is charged with an extra electron^{9,10,27} (see Fig. 1). The resulting coupling Hamiltonian, linear in the deflection X , reads

$$H_c = F_e X n_d. \quad (8)$$

Since the occupation of the quantum dot n_d (which varies in our model between 0 and 1) follows a Poissonian statistics, the coupling (8) results in a stochastic force which is exerted on the nanotube whenever the latter is charged with an extra electron. Such a coupling induces a blockade of the current at low bias voltage⁵ which can be dramatically enhanced at the Euler buckling instability.¹¹ Due to the backaction that the current flow exerts on the nanobeam, the coupling (8) further induces a renormalization of its vibrational frequency, as recently observed in suspended carbon nanotubes.^{9,10} For quantized high-energy vibrational modes, a linear electron-vibron coupling similar to Eq. (8), but not induced by the gate capacitance, leads to the Franck-Condon blockade.⁶⁻⁸

On top of the electrostatic potential (8), a second kind of coupling between the mechanical and electronic degrees of freedom stems from the electron-phonon coupling intrinsic to the tube and is quadratic in X .²⁵ As shown in Ref. 24, such a coupling leads to a current-induced discontinuous Euler instability and to a novel mechanism of current blockade at low bias voltage, termed “tricritical current blockade”. The relative importance of the two types of coupling mentioned above is controlled by the distance h between the nanobeam and the gate electrode. Indeed, the intrinsic coupling does not depend on h , while the strength of the gate-induced coupling (8) depends logarithmically on h .²⁷ In the remainder of this paper, we assume that the distance h is sufficiently small such that the coupling (8) dominates and thus neglect the intrinsic electron-phonon coupling.

III. CURRENT-INDUCED LANGEVIN DYNAMICS

The model encapsulated in the Hamiltonian (1) can be solved in an essentially exact way by noticing that close to the Euler instability, where $\omega \rightarrow 0$ [see Eq. (3)], (i) the vibrational mode is classical, $\hbar\omega \ll k_B T$ with T the temperature, and (ii) it is extremely slow as compared to the electronic dynamics, $\omega \ll \Gamma$, where Γ is the typical tunneling-induced width (or hybridization) of the energy level of the dot. Within a non-equilibrium Born-Oppenheimer approximation²⁸⁻³² which exploits the separation of timescales between fast electronic and slow vibrational degrees of freedom, and which is asymptotically exact at the buckling instability where $\omega \rightarrow 0$,^{11,24} the dynamics of the nanobeam is described by a Langevin

process with Gaussian white noise, equivalent³³ to the Fokker-Planck equation

$$\begin{aligned} \partial_t \mathcal{P} = & -\frac{P}{m} \partial_X \mathcal{P} - F_{\text{eff}}(X) \partial_P \mathcal{P} \\ & + \frac{\eta(X)}{m} \partial_P (P \mathcal{P}) + \frac{D(X)}{2} \partial_P^2 \mathcal{P} \end{aligned} \quad (9)$$

for the probability $\mathcal{P}(X, P, t)$ to find the resonator at phase-space point (X, P) at time t . The effective force

$$F_{\text{eff}}(X) = -m\omega^2 X - \alpha X^3 - F_e n_0(X) \quad (10)$$

can be easily inferred from averaging the Heisenberg equations of motion for X and P on a timescale long as compared to Γ^{-1} , but short relative to ω^{-1} . In Eq. (10), the term proportional to the average dot occupation for fixed X , $n_0(X) = \langle n_d \rangle_X$, corresponds to a conservative force that modifies the dynamical properties of the nanobeam in presence of a current flow. In Eq. (9), $\eta(X)$ and $D(X)$ represent a current-induced friction and fluctuation coefficient, respectively. These quantities can be expressed through the non-equilibrium lesser and greater Green’s functions of the dot at fixed X , $G_d^<(t, X) = i \langle d^\dagger d(t) \rangle_X$ and $G_d^>(t, X) = -i \langle d(t) d^\dagger \rangle_X$, respectively. One finds²⁸⁻³²

$$n_0(X) = -i \int \frac{d\epsilon}{2\pi\hbar} G_d^<(\epsilon, X), \quad (11a)$$

$$\eta(X) = F_e^2 \int \frac{d\epsilon}{2\pi\hbar} G_d^<(\epsilon, X) \partial_\epsilon G_d^>(\epsilon, X), \quad (11b)$$

$$D(X) = F_e^2 \int \frac{d\epsilon}{2\pi\hbar} G_d^<(\epsilon, X) G_d^>(\epsilon, X), \quad (11c)$$

with

$$\begin{aligned} G_d^<(\epsilon, X) &= \int dt e^{i\epsilon t/\hbar} G_d^<(t, X) \\ &= i\hbar^2 \frac{\sum_a \Gamma_a f_a(\epsilon)}{[\epsilon - \mathcal{E}_d(X)]^2 + (\hbar\Gamma/2)^2}, \end{aligned} \quad (12a)$$

$$\begin{aligned} G_d^>(\epsilon, X) &= \int dt e^{i\epsilon t/\hbar} G_d^>(t, X) \\ &= -i\hbar^2 \frac{\sum_a \Gamma_a [1 - f_a(\epsilon)]}{[\epsilon - \mathcal{E}_d(X)]^2 + (\hbar\Gamma/2)^2}. \end{aligned} \quad (12b)$$

In Eq. (12), we defined the Fermi function in lead a ,

$$f_a(\epsilon) = \frac{1}{\exp[(\epsilon - \mu_a)/k_B T] + 1}, \quad (13)$$

the effective dot energy for fixed X ,

$$\mathcal{E}_d(X) = \epsilon_d - e\bar{V}_g + F_e X, \quad (14)$$

and the hybridization $\Gamma = \sum_a \Gamma_a$ with $\Gamma_a = 2\pi |t_a|^2 \nu / \hbar$. Here, ν is the density of states in the leads, assumed to be constant.

The Fokker-Planck equation (9) can be conveniently rewritten using the relevant time, length and energy

scales of the problem, i.e., the vibrational frequency for vanishing compression force ω_0 [see Eq. (3)], the polaronic shift $\ell = F_e/m\omega_0^2$ and the corresponding energy $E_E^0 = F_e\ell$, respectively. Introducing the dimensionless position, momentum and time, $x = X/\ell$, $p = P/m\omega_0\ell$, and $\tau = \omega_0 t$, respectively, one obtains for Eq. (9)

$$\partial_\tau \mathcal{P} = -p\partial_x \mathcal{P} - f_{\text{eff}}(x)\partial_p \mathcal{P} + \gamma(x)\partial_p(p\mathcal{P}) + \frac{d(x)}{2}\partial_p^2 \mathcal{P}. \quad (15)$$

The scaled effective force

$$f_{\text{eff}}(x) = \delta x - \tilde{\alpha}x^3 - n_0(x) \quad (16)$$

is expressed in terms of the reduced compression force $\delta = F/F_c - 1$ and the scaled anharmonicity $\tilde{\alpha} = \alpha\ell^4/E_E^0$. In the low-temperature limit (or equivalently the strong coupling limit) $k_B T \ll \hbar\Gamma$, i.e., the cotunneling regime where resonant transport is fully coherent, the occupation of the dot for fixed deflection x , the (scaled) current-induced dissipation and fluctuation read^{29,31}

$$n_0(x) = \frac{1}{2} + \sum_a \frac{\gamma_a}{\pi} \arctan\left(\frac{\tilde{\mu}_a + v_g - x}{\tilde{\Gamma}/2}\right), \quad (17)$$

$$\gamma(x) = \frac{\tilde{\omega}_0 \tilde{\Gamma}^2}{4\pi} \sum_a \frac{\gamma_a}{[(\tilde{\mu}_a + v_g - x)^2 + (\tilde{\Gamma}/2)^2]}, \quad (18)$$

$$d(x) = \frac{2\gamma_L \gamma_R \tilde{\omega}_0}{\pi \tilde{\Gamma}} \sum_{a \neq b} \theta(\tilde{\mu}_a - \tilde{\mu}_b) \times \left[\arctan z + \frac{z}{1+z^2} \right] \frac{\tilde{\mu}_a + v_g - x}{\tilde{\Gamma}/2}, \quad (19)$$

respectively. We introduced the notation $\gamma_a = \Gamma_a/\Gamma$, $v_g = (e\tilde{V}_g - \epsilon_d)/E_E^0$, $\tilde{\mu}_L = -\tilde{\mu}_R = v/2$ with $v = eV/E_E^0$, $\tilde{\omega}_0 = \hbar\omega_0/E_E^0$, and $\tilde{\Gamma} = \hbar\Gamma/E_E^0$. Solving for the stationary solution of the Fokker-Planck equation (15), $\partial_\tau \mathcal{P}_{\text{st}} = 0$, one can calculate the average current through the device according to

$$I = \int dx dp \mathcal{I}(x) \mathcal{P}_{\text{st}}(x, p), \quad (20)$$

with

$$\mathcal{I}(x) = \frac{e\Gamma\gamma_L\gamma_R}{\pi} \left[\arctan\left(\frac{\tilde{\mu}_L + v_g - x}{\tilde{\Gamma}/2}\right) - \arctan\left(\frac{\tilde{\mu}_R + v_g - x}{\tilde{\Gamma}/2}\right) \right] \quad (21)$$

the quasi-stationary current for fixed x .

Before we proceed, we notice that for the experiment of Steele *et al.*⁹ on suspended carbon nanotubes, it was estimated in Ref. 11 that $E_E^0 \simeq 5 \mu\text{eV}$ and $\tilde{\alpha} \simeq 10^{-10}$, yielding $\tilde{\Gamma} \simeq 10$, $\tilde{\omega}_0 \simeq 0.1$, and a reduced temperature $\tilde{T} = k_B T/E_E^0 \simeq 1$. This experiment is thus in the low-temperature adiabatic regime which is investigated here where $\tilde{\omega}_0 \ll \tilde{T} \ll \tilde{\Gamma}$, and where cotunneling might play a

role on the transport characteristics. As for the similar experiments by Lassagne *et al.*¹⁰, $E_E^0 \simeq 5 \mu\text{eV}$ and $\tilde{\alpha} \simeq 10^{-8}$,¹¹ such that we have $\tilde{\Gamma} \simeq 0.5$, $\tilde{\omega}_0 \simeq 10^{-2}$ and $\tilde{T} \simeq 10^3$. The experiment of Ref. 10 is thus clearly in the high-temperature regime $\tilde{\omega}_0 \ll \tilde{\Gamma} \ll \tilde{T}$ where sequential transport dominates over cotunneling and which has been investigated in detail in Ref. 11.

IV. TRANSPORT CHARACTERISTICS OF THE DEVICE

We now turn to the study of the transport characteristics of the device of Fig. 1 with the approach detailed in Sec. III. We start in Sec. IV A with a mean-field approximation that neglects the current-induced dissipation (18) and fluctuation (19). We then consider the full non-equilibrium dynamics of the device in Sec. IV B before we investigate the effects of a finite quality factor of the nanobeam in Sec. IV C.

A. Mean-field approximation

It is first instructive to consider the limit $\tilde{\omega}_0 \rightarrow 0$ to understand the transport characteristics of the system. Within this limit, the current-induced dissipation (18) and fluctuation (19) can be neglected as compared to the effective force (16) entering the Fokker-Planck equation (15). In that case, any infinitesimally small extrinsic damping mechanism will, at zero temperature, localize the system at a deflection x corresponding to the global minimum x_m of the effective potential

$$v_{\text{eff}}(x) = -\frac{\delta x^2}{2} + \frac{\tilde{\alpha}x^4}{4} + \frac{x}{2} - \sum_a \frac{\gamma_a}{\pi} \left[(\tilde{\mu}_a + v_g - x) \arctan\left(\frac{\tilde{\mu}_a + v_g - x}{\tilde{\Gamma}/2}\right) - \frac{\tilde{\Gamma}}{4} \ln\left((\tilde{\mu}_a + v_g - x)^2 + (\tilde{\Gamma}/2)^2\right) \right] \quad (22)$$

associated to the effective force (16). Within this mean-field approximation, the stationary solution of the Fokker-Planck equation (15) is given by $\mathcal{P}_{\text{st}}(x, p) = \delta(x - x_m)\delta(p)$ such that the current (20) reduces to $I = \mathcal{I}(x_m)$, with $\mathcal{I}(x)$ the quasi-stationary current of Eq. (21).

The mechanism of the classical current blockade is encapsulated in the effective potential (22) and in the quasi-stationary current (21). Indeed, the effective potential (22) can, depending on the parameters, show up to five metastable minima. These positions x can either correspond to an effective dot energy level (14) located within the bias window, $\mathcal{E}_d(X) \leq e|V|/2$, where sequential tunneling dominates and where the current is maximal (“conducting” minima), either to positions such that $\mathcal{E}_d(X) > e|V|/2$ where cotunneling dominates and the current is algebraically suppressed on a scale given

by the hybridization Γ (“blocked” minima). For a given gate voltage, the system passes for increasing bias voltage from a stable position x_m corresponding to the cotunnel-

ing (blocked) region to a stable position where sequential tunneling dominates (conducting region), thus defining a bias voltage below which current is suppressed.

1. Limit of vanishing hybridization to the leads.

We start by considering the limit $\tilde{\Gamma} \rightarrow 0$ such that the dot occupation (17) simplifies to

$$n_0(x) = \begin{cases} 1, & x < v_g - \frac{|v|}{2}, \\ \gamma_L \Theta(v) + \gamma_R \Theta(-v), & v_g - \frac{|v|}{2} \leq x \leq v_g + \frac{|v|}{2}, \\ 0, & x > v_g + \frac{|v|}{2}, \end{cases} \quad (23)$$

where $\Theta(z)$ is the Heaviside step function. In that case, the dynamical equilibrium condition $f_{\text{eff}}(x) = 0$ and $df_{\text{eff}}/dx < 0$ with $f_{\text{eff}}(x)$ the effective force (16) determining the metastable positions of the system can be solved analytically. We find that the regions where current can flow are delineated in the v - v_g plane by straight lines $v \sim \pm 2v_g$. For $v > 0$, and to first order in the small parameter $\tilde{\alpha}^{1/3}/|\delta|$ ($|\delta|/\tilde{\alpha}^{1/3}$) far (close) to the buckling instability, the apex of the resulting conducting region defines a gap Δ_v below which transport is blocked,

$$\Delta_v = \begin{cases} -\frac{1}{2\delta}, & -\delta \gg \tilde{\alpha}^{1/3}, \\ \frac{1}{4\delta}, & \delta \gg \tilde{\alpha}^{1/3}, \\ \frac{1}{2\tilde{\alpha}^{1/3}\gamma_R} \left[\frac{3}{2} (1 - \gamma_L^{1/3}) + \frac{\delta}{\tilde{\alpha}^{1/3}} (1 - \gamma_L^{-1/3}) \right], & |\delta| \ll \tilde{\alpha}^{1/3}. \end{cases} \quad (24)$$

The gate voltage at which one obtains the minimal threshold (24) reads

$$v_g^{\min} = \begin{cases} \frac{\gamma_L + 1/2}{2\delta}, & -\delta \gg \tilde{\alpha}^{1/3}, \\ -\frac{\gamma_L + 1/2}{4\delta} - \sqrt{\frac{\delta}{\tilde{\alpha}}}, & \delta \gg \tilde{\alpha}^{1/3}, \\ -\frac{1}{8\tilde{\alpha}^{1/3}\gamma_R} \left\{ 3 \left[1 + \gamma_L^{1/3}(\gamma_R - \gamma_L) \right] + \frac{2\delta}{\tilde{\alpha}^{1/3}} \left[1 + \gamma_L^{-1/3}(\gamma_R - \gamma_L) \right] \right\}, & |\delta| \ll \tilde{\alpha}^{1/3}. \end{cases} \quad (25)$$

The case $v < 0$ is easily obtained by swapping L and R in Eqs. (24) and (25).

The regions in the v - v_g plane where current can flow through the nanobeam are shown in Fig. 2 in red/dark gray. As it is the case in the sequential-tunneling regime,¹¹ the current blockade characterized by the gap (24) increases for increasing compression force $\delta < 0$ below the mechanical instability [see Figs. 2(a) and 2(b)]. The gap is maximal at the Euler buckling instability where $\delta = 0$ [see Fig. 2(c)] before it decreases above the instability [$\delta > 0$, see Figs. 2(d) and 2(e)]. Since $\tilde{\alpha} \ll 1$,¹¹ Δ_v is orders of magnitude larger than away from the mechanical instability. Moreover, one observes in Fig. 2 a shift of the tip of the conducting regions for positive and negative bias voltages which is due to the

asymmetry of the coupling to the left and right leads ($\gamma_L \neq \gamma_R$). Indeed, this shift which is maximal at the buckling instability [Fig. 2(c)] can be traced back to the different occupations of the dot for fixed x [Eq. (23)] for positive and negative biases when x is such that the effective energy level of the dot (14) belongs to the sequential-tunneling region. Such an asymmetry of the conducting regions for positive and negative bias voltages has also been observed experimentally in suspended carbon nanotubes for quantized vibrational modes⁸ and is thus not specific to the classical regime considered here.

We conclude this section by noticing that the limit $\tilde{\Gamma} \rightarrow 0$ presented here is quantitatively similar to the zero-temperature mean-field limit considered in Ref. 11 where sequential transport and symmetric coupling to

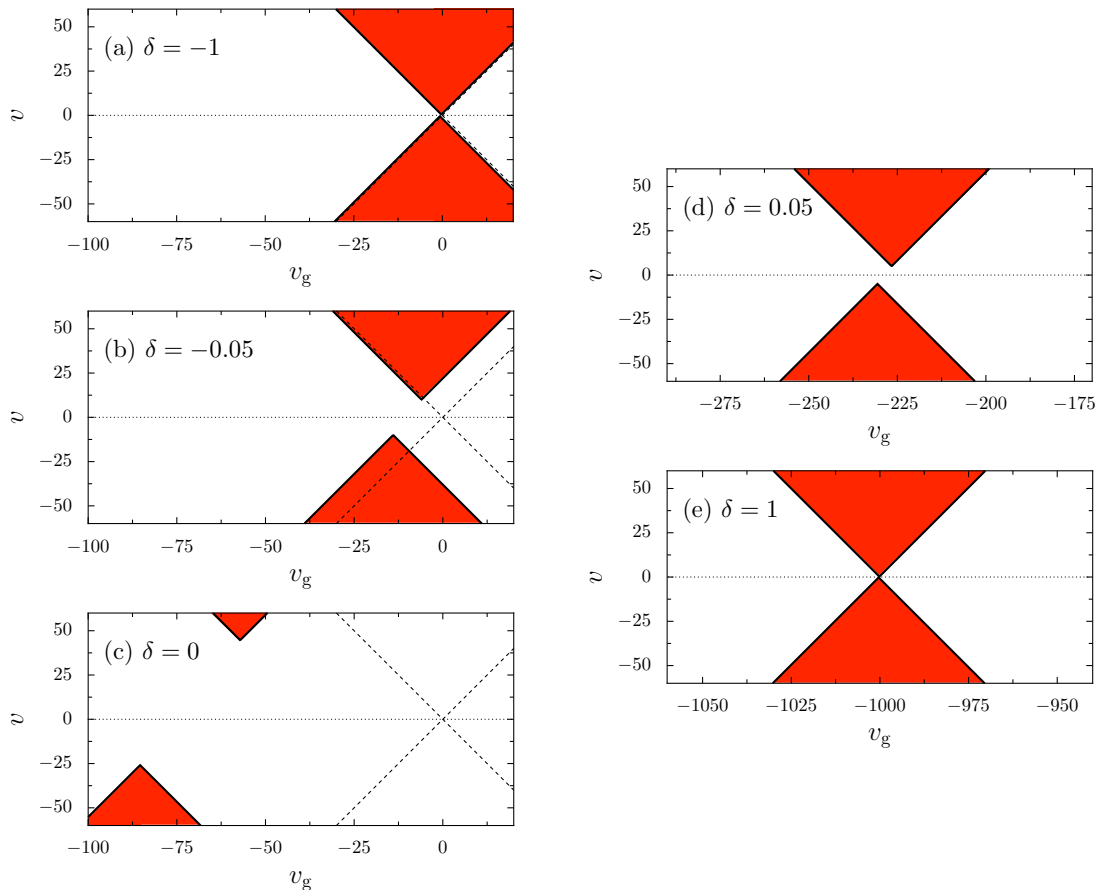


FIG. 2. (Color online) Conducting regions at mean-field level (in red/dark gray) in the v - v_g plane for $\tilde{\Gamma} \rightarrow 0$. The red/dark gray and white areas correspond to a current $|I| = e\Gamma\gamma_L\gamma_R$ and $I = 0$, respectively. The scaled compression force δ increases from (a) to (e). In the figure, $\gamma_L = 0.1$, $\gamma_R = 1 - \gamma_L = 0.9$ and $\tilde{\alpha} = 10^{-6}$. The dashed lines indicate the delimitation of the conducting regions for vanishing electromechanical coupling ($F_e = 0$).

the leads were assumed, as the effective potential $v_{\text{eff}}(x)$ has the same functional form in both cases [compare Eqs. (24) and (25) above for $\gamma_L = \gamma_R = 1/2$ with Eqs. (23) and (24) in Ref. 11]. Hence, the enhancement of the current blockade is, at mean-field level, not specific to the transport regime considered.

2. Finite hybridization to the leads.

At finite $\tilde{\Gamma}$, we search for the global minimum of the effective potential (22) numerically. The resulting average current is shown in Fig. 3 as a function of the bias voltage for gate voltages corresponding to the apex of the conducting region, $v_g = v_g^{\text{min}}$ [cf. Eq. (25)]. One finds that the current behavior, plotted as a function of v/Δ_v , is similar for a given $\tilde{\Gamma}/\Delta_v$ at the instability [Fig. 3(a)] and away from the instability [Fig. 3(b)]. As the hybridization $\tilde{\Gamma}$ is increased, the low-bias current blockade becomes less pronounced since cotunneling becomes dominant in the blocked region ($v < \Delta_v$). For $\tilde{\Gamma} \gg \Delta_v$ (red dotted

line), the blockade completely disappears. In that limit, one recovers the usual linear-response current in absence of electromechanical coupling ($F_e = 0$), $I = 4\gamma_L\gamma_R G_0 V$, with $G_0 = e^2/2\pi\hbar$ the conductance quantum. The results of Fig. 3 show (at mean-field level) that it is advantageous to tune the system at the Euler instability, where the gap Δ_v dramatically increases [see Eq. (24)] such that the blockade is much more pronounced for a given hybridization $\tilde{\Gamma}$ to the leads.

B. Non-equilibrium dynamics

We now turn to the role played by the current-induced dissipation (18) and fluctuations (19) on the current blockade by considering the case $\tilde{\omega}_0 \neq 0$. To this end, we solve for the stationary solution of the Fokker-Planck equation (15) numerically as described in Ref. 29. In what follows, we focus on the system at the Euler instability ($\delta = 0$) where the current blockade is, at mean-field level, maximal [cf. Eq. (24)]. Since the stationary solu-

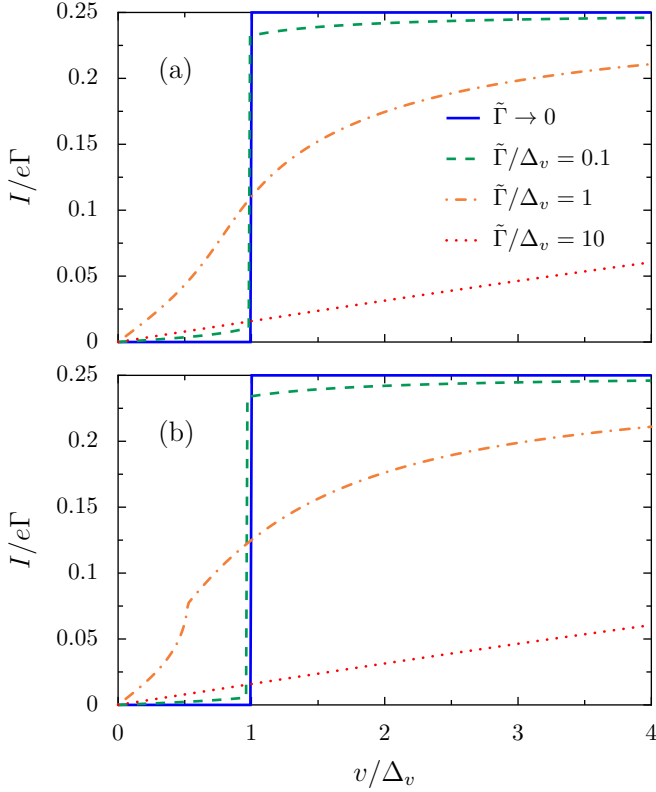


FIG. 3. (Color online) Mean-field current I as a function of bias v scaled by the gap (24) for a gate voltage $v_g = v_g^{\min}$ corresponding to the apex of the conducting region, see Eq. (25). (a) Compression force $\delta = 0$ corresponding to the Euler instability. (b) Compression forces $|\delta| \gg \tilde{\alpha}^{1/3}$ far from the buckling instability. In the figure, symmetric coupling to the leads is considered ($\gamma_L = \gamma_R = 1/2$).

tion of the Fokker-Planck equation (15) is, for $\tilde{\omega}_0 \ll 1$, independent of the actual value of $\tilde{\omega}_0$ (see appendix E in Ref. 11 for details), we set $\tilde{\omega}_0 = 10^{-3}$ in what follows.

Our results for the average current are shown in Fig. 4(a) for increasing hybridization to the leads $\tilde{\Gamma}$ which controls the range of the current-induced dissipation (18) and fluctuations (19). For $\tilde{\Gamma}$ smaller than the energy gap Δ_v (see green squares and orange circles in the figure), the current-induced fluctuations have a dramatic effect on the I - V characteristics for bias voltages larger than Δ_v [compare with the mean-field results of Fig. 3(a), green dashed and orange dashed-dotted lines]. However, for $\tilde{\Gamma} \leq 0.1\Delta_v$ and $v < \Delta_v$, cotunneling does not suppress the current blockade at low bias. We expect that for smaller $\tilde{\Gamma}$ (which is numerically very difficult to tackle), the current blockade should be even more pronounced. As close to the mechanical instability, the gap (24) is very large, we foresee that the current blockade should be clearly visible in an experiment even in the regime of strong coupling to the electron reservoirs where cotunneling can be significant.

The above results are confirmed by the behavior of the differential conductance dI/dV shown in Fig. 4(b):

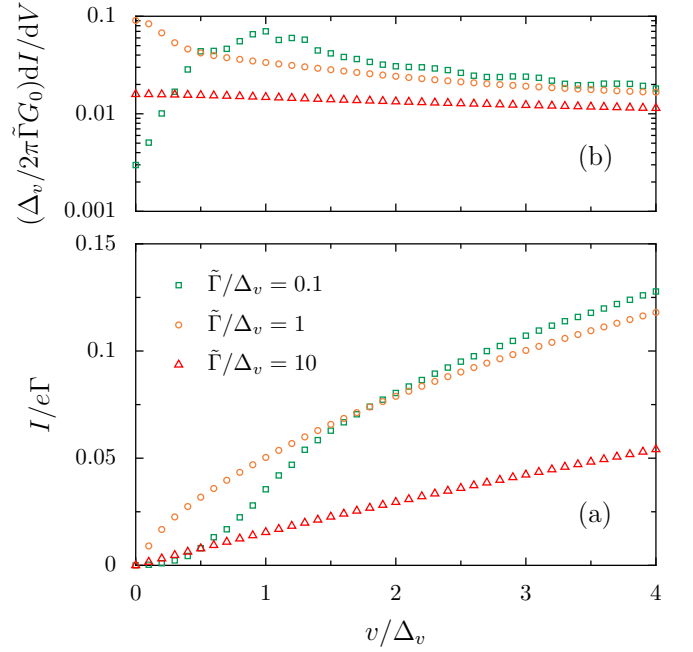


FIG. 4. (Color online) (a) Current I including the nonequilibrium Langevin dynamics as a function of bias v at the Euler buckling instability ($\delta = 0$) for a gate voltage $v_g = v_g^{\min}$ corresponding to the apex of the conducting region, see Eq. (25). (b) Corresponding differential conductance dI/dV , where $G_0 = e^2/2\pi\hbar$ denotes the conductance quantum. In the figure, symmetric coupling to the leads is considered ($\gamma_L = \gamma_R = 1/2$), $\tilde{\alpha} = 10^{-6}$ and $\tilde{\omega}_0 = 10^{-3}$.

For a hybridization to the leads small as compared to the energy gap (green squares in the figure), the differential conductance is clearly suppressed at low bias voltage, while for larger $\tilde{\Gamma}$, the conductance acquires a finite value which is almost constant as a function of the bias voltage [orange circles and red triangles in Fig. 4(b)].

C. Role of extrinsic dissipation

Nanoelectromechanical systems are subject to various sources of extrinsic dissipation that leads to a finite quality factor Q of the nanobeam that we have ignored so far. These mechanisms of extrinsic dissipation come from localized defects at the surface of the sample,^{34–36} clamping and thermoelastic losses,³⁷ Ohmic losses due to the gate electrode,³⁸ etc. Within the Caldeira-Leggett model and assuming Ohmic (memory-free) dissipation,³⁹ one can easily incorporate these mechanisms in the Fokker-Planck equation (15) by replacing $\gamma(x) \rightarrow \gamma(x) + \gamma_e$ and $d(x) \rightarrow d(x) + 2\gamma_e \tilde{T}$, with $\gamma_e = Q^{-1}$ the extrinsic damping constant (or inverse quality factor) and $\tilde{T} = k_B T / E_E^0$ the (reduced) temperature.

Numerical results for various values of the ratio $\gamma_e/\tilde{\omega}_0$ are shown for the current in Fig. 5(a) and for the corresponding differential conductance in Fig. 5(b). The

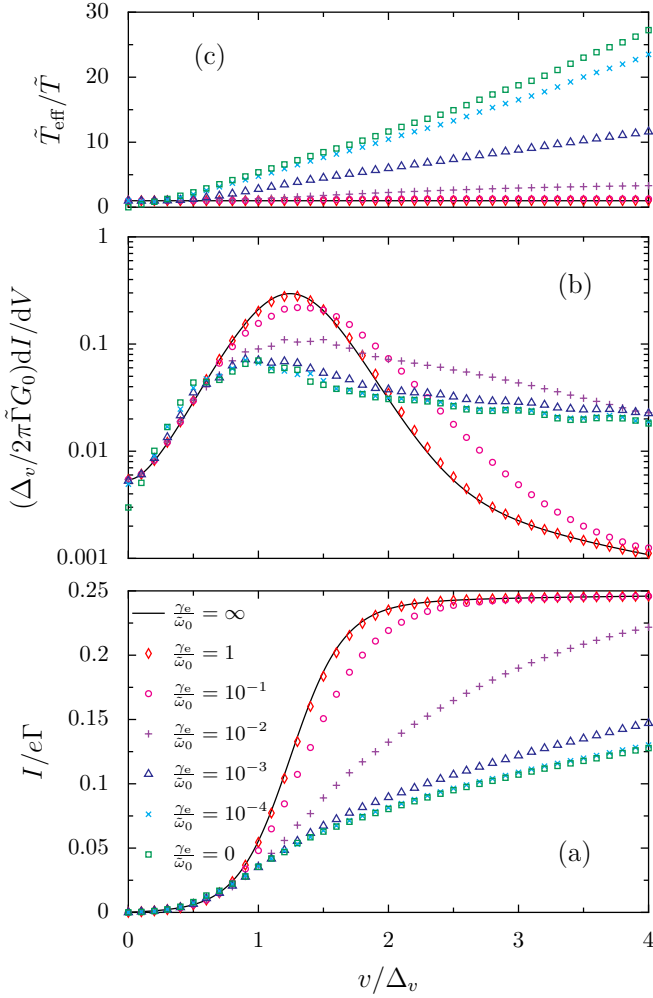


FIG. 5. (Color online) (a) Average current and (b) differential conductance as a function of the bias voltage at the Euler buckling instability ($\delta = 0$) for various values of the extrinsic damping constant γ_e . (c) Corresponding effective temperature \tilde{T}_{eff} defined in Eq. (26). In the figure, $\tilde{\alpha} = 10^{-6}$, $\tilde{\omega}_0 = 10^{-3}$, $\tilde{\Gamma}/\Delta_v = 0.1$, $\tilde{T}/\Delta_v = 0.05$, $\gamma_L = \gamma_R = 1/2$, and the gate voltage corresponds to the apex of the conducting region, see Eq. (25).

parameter $\gamma_e/\tilde{\omega}_0$ measures the relative importance of the two sources of fluctuations, i.e., thermal vs. current-induced [cf. Eqs. (18) and (19)], from vanishing extrinsic dissipation [green squares in Figs. 5(a) and 5(b)] to purely thermal fluctuations (solid line in the figure), where the probability $\mathcal{P}_{\text{st}}(x, p)$ entering Eq. (20) obeys a Boltzmann distribution at temperature \tilde{T} . We can conclude from the results of Figs. 5(a) and 5(b) that the larger the extrinsic dissipation (or the smaller the quality factor), the more pronounced is the current blockade. As it is the case in the sequential-tunneling regime,¹¹ the extrinsic dissipation helps localizing the system at phase-space points corresponding to the metastable minima of the effective potential (22), rendering the current blockade sharper. The same conclusion holds for quantized vibrations, where

the Franck-Condon blockade is more pronounced for fast equilibration of the vibronic mode.^{6,7}

The results for the average current in Fig. 5(a) and for the differential conductance in Fig. 5(b) can be interpreted in terms of an effective temperature

$$\tilde{T}_{\text{eff}} = \frac{\langle d \rangle / 2 + \gamma_e \tilde{T}}{\langle \gamma \rangle + \gamma_e} \quad (26)$$

defined in analogy with the fluctuation-dissipation theorem,³³ where

$$\langle \gamma \rangle = \int dx dp \gamma(x) \mathcal{P}_{\text{st}}(x, p) \quad (27)$$

and

$$\langle d \rangle = \int dx dp d(x) \mathcal{P}_{\text{st}}(x, p) \quad (28)$$

are the averages over phase-space of the current-induced dissipation (18) and fluctuation (19), respectively. As one can see in Fig. 5(c), \tilde{T}_{eff} almost equals the electronic temperature \tilde{T} for inverse quality factors γ_e of the order of $\tilde{\omega}_0$, thus explaining why the current and conductance behavior are similar to the case where only thermal fluctuations are present [compare red diamonds and magenta circles with the solid line in Figs. 5(a) and 5(b)]. For smaller γ_e (larger quality factors Q), the effective temperature becomes significantly larger than \tilde{T} and increases with increasing bias voltage. Hence, the mechanical system fluctuates more in phase-space and switches back and forth between minima of the effective potential (22) corresponding to regions where the current at fixed x , Eq. (21), is suppressed (cotunneling/“blocked” regions) or enhanced (sequential tunneling/“conducting” regions), thus reducing the average current I and rendering the current blockade less pronounced.

We conclude this section on the transport characteristics of the device by noticing that the features of the classical current blockade in the vicinity of a mechanical instability are qualitatively the same in the sequential-tunneling and cotunneling transport regimes. In the former case, the electronic temperature defines the relevant energy scale below which the current blockade is observable,¹¹ while in the latter case, it is the hybridization to the electron reservoirs that plays a similar role. The enhancement of the current blockade at the Euler instability is thus a universal phenomenon that does not depend on the transport regime one considers.

V. BACKACTION OF THE CURRENT FLOW ON THE NANORESONATOR

A characteristic of nanoelectromechanical systems is the backaction that the current flow exerts on the mechanical part of the device. The current-induced force $-n_0(x)$ in the effective force (16) can indeed renormalize the nanobeam frequency. Since this current-induced

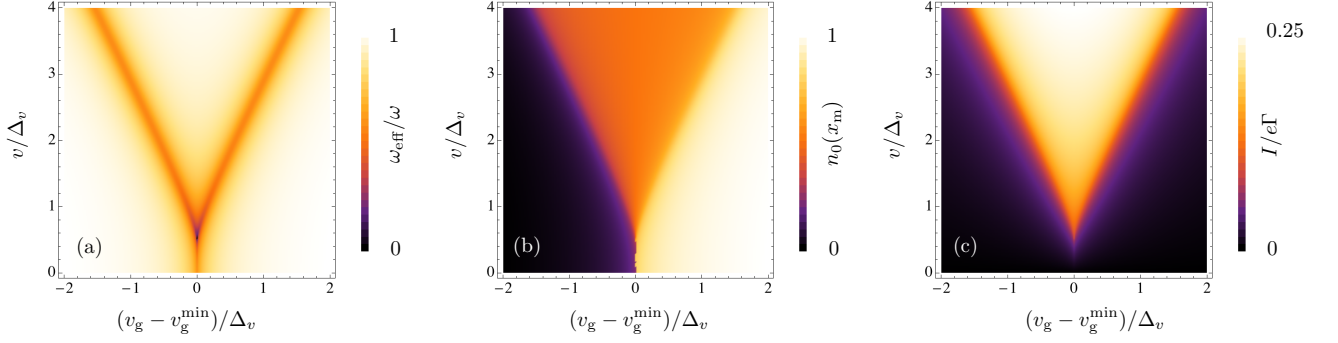


FIG. 6. (Color online) (a) Effective frequency ω_{eff} , (b) average occupation of the dot and (c) average current I as a function of bias voltage v and gate voltage v_g for compression forces far below the Euler instability ($-\delta \gg \tilde{\alpha}^{1/3}$). In the figure, $\tilde{\Gamma} = \Delta_v$ and $\gamma_L = \gamma_R = 1/2$.

force depends on the bias and gate voltages through the average occupation of the dot for fixed position x , one expects a strong signature of electronic transport on the nanobeam frequency.

In what follows, we quantify the current-induced effective frequency ω_{eff} of the nanobeam by the curvature of the effective potential (22) at its global minimum x_m , $\omega_{\text{eff}} = \omega_0 \sqrt{v''_{\text{eff}}(x_m)}$. Using Eqs. (16) and (17), we have

$$\omega_{\text{eff}} = \omega_0 \sqrt{-\delta + 3\tilde{\alpha}x_m^2 - \frac{\partial n_0}{\partial v_g} \bigg|_{x_m}}. \quad (29)$$

Since $\partial n_0 / \partial v_g > 0$, this expression shows that the nanobeam frequency will be significantly lowered when the average number of electrons on the dot varies as a function of gate voltage. This is illustrated in Figs. 6(a) and 6(b) where we show ω_{eff} and the average number of electrons on the dot n_0 as a function of bias v and gate voltage v_g , respectively, for intermediate hybridization to the leads $\tilde{\Gamma} = \Delta_v$. For bias voltages $v \lesssim \Delta_v$, the average occupation of the dot in Fig. 6(b) jumps from 0 to 1 around a gate voltage corresponding to Eq. (25) and on a scale given by the coupling to the leads $\tilde{\Gamma}$, resulting in a renormalization of the nanobeam frequency along the line $v_g = v_g^{\text{min}}$, see Fig. 6(a). For $v \gtrsim \Delta_v$, the frequency is mostly renormalized for gate voltages corresponding to the borders between the sequential tunneling region (where $n_0 \simeq 1/2$) and the cotunneling regions (where $n_0 \simeq 0$ or 1). This is further illustrated in Fig. 6(c) which shows the corresponding average current flowing through the nanobeam. The results of Fig. 6 are obtained for compression forces $-\delta \gg \tilde{\alpha}^{1/3}$, i.e., far below the Euler instability. Far above the instability ($\delta \gg \tilde{\alpha}^{1/3}$), the results of Fig. 6 remain unchanged, except that one has to replace $\omega_{\text{eff}}/\omega$ by $\omega_{\text{eff}}/\sqrt{2}|\omega|$ in Fig. 6(a) since in the buckled state, the vibrational frequency squared in absence of a current flow is twice as much as in the flat state, see Eq. (29).

In Fig. 7, we study the influence of the hybridization $\tilde{\Gamma}$ on the current-induced frequency shift. We show in the figure the effective frequency ω_{eff} as a function of the

bias voltage for gate voltages corresponding to the apex of the conducting region [cf. Eq. (25)], for compression forces far below the Euler instability ($-\delta \gg \tilde{\alpha}^{1/3}$), and for various values of the hybridization $\tilde{\Gamma}$ to the leads. It is remarkable that for $\tilde{\Gamma} \rightarrow 0$ (thick black dotted line in Fig. 7), $\omega_{\text{eff}} = \omega$, i.e., there is no effect of the current flow on the vibrational frequency of the beam [since in that limit, the curvatures of the effective potential (22) is the same in all three metastable minima], while the current blockade is the most pronounced [see blue solid line in Fig. 3(b)]. For $\tilde{\Gamma} \gg \Delta_v$, the effective frequency $\omega_{\text{eff}}/\omega \simeq 1 - 2\Delta_v/\pi\tilde{\Gamma}$ is slightly reduced as compared to its value without a current flow and is independent of the bias voltage (see thick dashed line in Fig. 7). Only for $\tilde{\Gamma} \sim \Delta_v$ (see thin lines in Fig. 7) the beam experiences large bias-dependent frequency shifts due to the current flow, that can reach up to almost 100 % (see red solid line in the figure). This is in stark contrast with the behavior of the current [Fig. 3(b)], where the low-bias current blockade already almost disappears for intermediate values of the

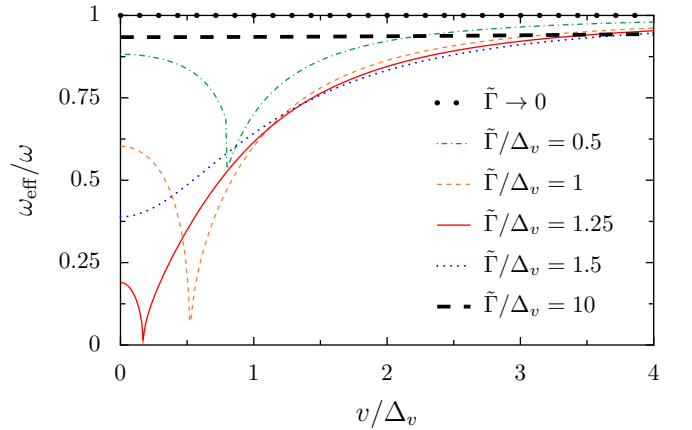


FIG. 7. (Color online) Effective frequency ω_{eff} of the nanobeam far below the Euler instability ($-\delta \gg \tilde{\alpha}^{1/3}$) as a function of bias voltage at the apex of the conducting region, $v_g = v_g^{\text{min}}$. In the figure, $\gamma_L = \gamma_R = 1/2$.

hybridization [see orange dashed-dotted line in Fig. 3(b)].

The results above show that, although the current blockade might not be experimentally accessible far below (or above) the Euler instability for intermediate hybridization to the leads, the current-induced frequency shift is considerably easier to detect. This was recently demonstrated experimentally on suspended carbon nanotubes,^{9,10} where despite the fact that the current blockade could not be detected due to the relatively weak electromechanical coupling encountered in experiments, a clear current-induced frequency shift was measured.

VI. CONCLUSION

In conclusion, we have analyzed the role played by cotunneling, relevant in the transport regime of strong hybridization to the electron reservoirs, on the low-bias current blockade in suspended single-electron transistors. We have shown that the dramatic enhancement at the Euler buckling instability of the bias voltage below which transport is suppressed predicted in Ref. 11 is not ruled out by cotunneling currents. The same conclusion holds in molecular devices for the Franck-Condon blockade in

the quantum regime.⁷ While in the sequential-tunneling regime, the temperature sets the limit of observability of the current blockade, it is the hybridization to the leads that plays a role qualitatively similar to the temperature when transport is fully coherent. The mechanism of the classical current blockade and of its enhancement in the vicinity of a mechanical instability is thus a universal feature of capacitively-coupled nanoelectromechanical systems, which does not qualitatively depend on the transport regime.

We have further studied the effect of backaction forces on the mechanical properties of the nanobeam. We have shown that the mechanical frequency can be strongly renormalized as a function of the bias voltage due to the force that is exerted by the current flow on the nanobeam. This effect might be considerably easier to observe than the current blockade when the system is far from the Euler buckling instability.

ACKNOWLEDGMENTS

We acknowledge Felix von Oppen, Fabio Pistolesi and Dietmar Weinmann for helpful comments and discussions.

-
- * Guillaume.Weick@ipcms.unistra.fr
- ¹ H. G. Craighead, *Science* **290**, 1532 (2000).
 - ² M. L. Roukes, *Phys. World* **14**, 25 (2001).
 - ³ K. L. Ekinci and M. L. Roukes, *Rev. Sci. Instrum.* **76**, 061101 (2005).
 - ⁴ M. Poot and H. S. J. van der Zant, e-print [arXiv:1106.2060v1](https://arxiv.org/abs/1106.2060v1) (unpublished).
 - ⁵ F. Pistolesi and S. Labarthe, *Phys. Rev. B* **76**, 165317 (2007).
 - ⁶ J. Koch and F. von Oppen, *Phys. Rev. Lett.* **94**, 206804 (2005).
 - ⁷ J. Koch, F. von Oppen, and A. V. Andreev, *Phys. Rev. B* **74**, 205438 (2006).
 - ⁸ R. Leturcq, C. Stampfer, K. Inderbitzin, L. Durrer, C. Hierold, E. Mariani, M. G. Schultz, F. von Oppen, and K. Ensslin, *Nat. Phys.* **5**, 327 (2009).
 - ⁹ G. A. Steele, A. K. Hüttel, B. Witkamp, M. Poot, H. B. Meerwaldt, L. P. Kouwenhoven, and H. S. J. van der Zant, *Science* **325**, 1103 (2009).
 - ¹⁰ B. Lassagne, Y. Tarakanov, J. Kinaert, D. Garcia-Sanchez, and A. Bachtold, *Science* **325**, 1107 (2009).
 - ¹¹ G. Weick, F. von Oppen, and F. Pistolesi, *Phys. Rev. B* **83**, 035420 (2011).
 - ¹² L. D. Landau and E. M. Lifshitz, *Theory of Elasticity* (Pergamon Press, Oxford, 1970).
 - ¹³ L. Euler in *Leonhard Euler's Elastic Curves*, translated and annotated by W. A. Oldfather, C. A. Ellis, and D. M. Brown, reprinted from ISIS, No. 58 XX(1) (Saint Catherine Press, Bruges, 1744).
 - ¹⁴ M. R. Falvo, G. J. Harris, R. M. Taylor II, V. Chi, F. P. Brooks Jr, S. Washburn, and R. Superfine, *Nature* **389**, 582 (1997).
 - ¹⁵ P. Poncharal, Z. L. Wang, D. Ugarte, and W. A. de Heer, *Science* **283**, 709 (1999).
 - ¹⁶ S. M. Carr and M. N. Wybourne, *Appl. Phys. Lett.* **82**, 709 (2003).
 - ¹⁷ S. M. Carr, W. E. Lawrence, and M. N. Wybourne, *Europhys. Lett.* **69**, 952 (2005).
 - ¹⁸ D. Roodenburg, J. W. Spronck, H. S. J. van der Zant, and W. J. Venstra, *Appl. Phys. Lett.* **94**, 183501 (2009).
 - ¹⁹ S. M. Carr, W. E. Lawrence, and M. N. Wybourne, *Phys. Rev. B* **64**, 220101(R) (2001).
 - ²⁰ P. Werner and W. Zwerger, *Europhys. Lett.* **65**, 158 (2004).
 - ²¹ V. Peano and M. Thorwart, *New J. Phys.* **8**, 21 (2006).
 - ²² S. Savel'ev, X. Hu, and F. Nori, *New J. Phys.* **8**, 105 (2006).
 - ²³ S. Savel'ev, A. L. Rakhmanov, X. Hu, A. Kasumov, and F. Nori, *Phys. Rev. B* **75**, 165417 (2007).
 - ²⁴ G. Weick, F. Pistolesi, E. Mariani, and F. von Oppen, *Phys. Rev. B* **81**, 121409(R) (2010).
 - ²⁵ E. Mariani and F. von Oppen, *Phys. Rev. B* **80**, 155411 (2009).
 - ²⁶ In the different context of a compressed rod embedded in an elastic medium, a discontinuous buckling instability was predicted at the classical level in S. Savel'ev and F. Nori, *Phys. Rev. B* **70**, 214415 (2004).
 - ²⁷ S. Sapmaz, Y. M. Blanter, L. Gurevich, and H. S. J. van der Zant, *Phys. Rev. B* **67**, 235414 (2003).
 - ²⁸ D. Mozyrsky, M. B. Hastings, and I. Martin, *Phys. Rev. B* **73**, 035104 (2006).
 - ²⁹ F. Pistolesi, Y. M. Blanter, and I. Martin, *Phys. Rev. B* **78**, 085127 (2008).
 - ³⁰ R. Hussein, A. Metelmann, P. Zedler, and T. Brandes, *Phys. Rev. B* **82**, 165406 (2010).
 - ³¹ A. Nocera, C. A. Perroni, V. Marigliano Ramaglia, and V.

- Cataudella, [Phys. Rev. B **83**, 115420 \(2011\)](#).
- ³² N. Bode, S. V. Kusminskiy, R. Egger, and F. von Oppen, [Phys. Rev. Lett. **107**, 036804 \(2011\)](#).
- ³³ R. Zwanzig, *Nonequilibrium Statistical Mechanics* (Oxford University Press, Oxford, 2001).
- ³⁴ P. Mohanty, D. A. Harrington, K. L. Ekinici, Y. T. Yang, M. J. Murphy, and M. L. Roukes, [Phys. Rev. B **66**, 085416 \(2002\)](#).
- ³⁵ C. Seoanez, F. Guinea, and A. H. Castro Neto, [EPL **78**, 60002 \(2007\)](#).
- ³⁶ C. Seoanez, F. Guinea, and A. H. Castro Neto, [Phys. Rev. B **77**, 125107 \(2008\)](#).
- ³⁷ A. N. Cleland, *Foundations of Nanomechanics* (Springer-Verlag, Berlin, 2003).
- ³⁸ C. Seoanez, F. Guinea, and A. H. Castro Neto, [Phys. Rev. B **76**, 125427 \(2007\)](#).
- ³⁹ U. Weiss, *Quantum Dissipative Systems* (World Scientific, Singapore, 1993).